Computationally Efficient Calculation of Aerodynamic Flows

Diego Alonso, José M. Vega, and Ángel Velázquez

***Abstract*—A method is presented to construct computationally efficient reduced order models (ROMs) of three dimensional aerodynamic flows around commercial aircraft components. The method is based on the proper orthogonal decomposition (POD) of a set of steady snapshots, which are calculated using an industrial computational fluid dynamics (CFD) solver. The POD-mode amplitudes are calculated minimizing a residual defined from the Euler equations, which makes the ROM independent of the peculiarities of the CFD solver. Also, both POD modes and the residual are calculated using only a limited number of points in the computational mesh. In spite of these simplifications, the method provides quite good approximations of the flow variables distribution in the whole computational domain, including the boundary layer and the wake. The method is tested considering the aerodynamic flow around a horizontal tail plane in the transonic range and proves to be robust and efficient.**

***Index Terms*—Reduced order models, proper orthogonal decomposition, aerodynamic flows.**

I. Introduction

AERODYNAMIC design and certification are crucial steps in product development. Improving designs and reducing cost and time to market are increasingly needed in aeronautics to survive in increasingly competitive global market scenarios. Although, a trend is observed to substitute wind tunnel tests by computational fluid dynamics (CFD) simulations, the huge computational resources and CPU time required to calculate a single simulation (about two CPU days for a commercial aircraft) makes this solution impractical. Thus, reducing computational time of CFD solvers is becoming the key step to facilitate their industrial use. ROMs are good candidates to fulfill this objective.

Broadly speaking, fluid dynamics ROMs are constructed expanding the flow variables in terms of the most energetic POD modes, calculated from a set of representative CFD computed snapshots. The associated mode amplitudes are calculated either solving a set of ordinary differential equations obtained upon Galerkin projection, or minimizing a predefined residual error. Examples of the former can be found in, *e.g.*, the articles by Galletti *et al* [1], Sirisup and Karniadakis [2], Burkhard *et al* [3], and Rapun and Vega [4], and examples of the latter, in the articles by LeGresley and Alonso [5], Alonso *et al* [6], and Rouizi *et al* [7], and Bache *et al* [8]. In both cases, the CPU time needed to compute the ROM is much smaller than the CPU time required to run the CFD solver.

Manuscript received March 7, 2011; revised March 28, 2011. This work was partially supported by the Spanish Ministry of Science and Technology, under Grants DPI2009-07591 and TRA 2010-18054.

D. Alonso and A. Velazquez are in the Aerospace Propulsion and Fluid Mechanics Department, School of Aeronautics, Universidad Politécnica de Madrid, Spain, e-mail: diego.alonso.fernandez@upm.es, angel.velazquez@upm.es.

J.M. Vega is in the Applied Mathematics Department, School of Aeronautics, Universidad Politécnica de Madrid, Spain, e-mail: josemanuel.vega@upm.es.

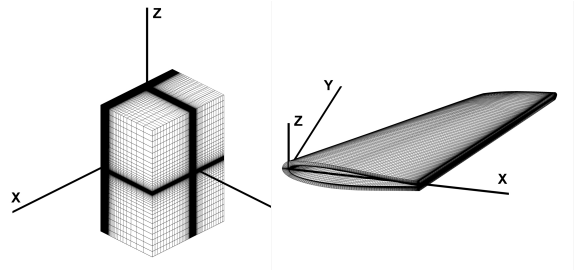

Fig. 1. Three dimensional views of the whole computational mesh (left) and the HTP with the O-mesh (rigth).

In this paper we present a robust ROM of multiparameter, three dimensional, steady, aerodynamic flows based on the minimizaction of a properly defined residual. For illustration, the method will be applied to calculate the aerodynamic flow around a HTP, which will be kept in mind in the description of the method.

II. CFD calculation of the snapshots and POD modes

The ROM that will be derived in the paper will be illustrated considering the aerodynamic flow around a three-dimensional HTP (Fig.1, right), depending on two parameters, the angle of attack and the Mach number, in the range $-3.0^\circ \leq AoA \leq 3.0^\circ$ and $0.4 \leq M \leq 0.8$; see Fig.2 below. The flow around the HTP in such range presents strong shock waves that move only slightly as the parameters are varied. This means that no special shock wave treatment is needed, unlike the case studied by Alonso *et al.* [9]

Snapshots will be calculated using the ELSA code [10], [11], developed by ONERA and CERFACS, which is a finite volume discretization [12] of the compressible continuity, momentum, and energy equations, with viscous terms modified according to an Edwards-corrected [13] Spalart-Almaras turbulence model [14] and some extra stabilizing terms added for numerical reasons. Further details of the numerical solver itself will not been needed below to develop the ROM.

The HTP has a span length 1.5 times its root chord, c. The position and orientation of the Cartesian coordinate frame is sketched in Fig.1. The complete computational mesh (Fig.1, left) is structured, with a total number of 3,053,744 mesh points in a parallelepipedic computational domain of sides $-5c < x < 10c$, $0 < y < 10c$, and $-10c < z < 10c$. Those blocks that are adjacent to the HTP surface build what will be called the O-mesh (Fig. 1, right), whose wall normal size

ISBN: 978-988-19251-5-2
ISSN: 2078-0958 (Print); ISSN: 2078-0966 (Online)

is comparable to the HTP thickness. Mesh points concentrate in the O-mesh, which contains 840,825 mesh points. In fact, the ROM will be constructed using only a part of the O-mesh (to both calculate the POD modes and project the governing equations) and a few points in the plane $x = -5c$ plane (to impose the upstream boundary conditions), which are

$$\begin{aligned} BC_1 &\equiv \rho u - M\cos AoA = 0, \\ BC_2 &\equiv \rho w - M\sin AoA = 0, \\ BC_3 &\equiv \rho v, \quad BC_4 \equiv \rho - 1 = 0, \\ BC_5 &\equiv p - 1 = 0. \end{aligned} \tag{1}$$

in terms of the flow variables, which (after substituting substituting the equation of state for ideal gases) are the mass fluxes in the x, y, and z directions, ρu, ρv, and ρw, the density, and the pressure, nondimensionalized using their respective upstream values.

The flow variables $q = (\rho u, \rho v, \rho w, \rho, p)$ are written as expansions in the POD-modes, as

$$\mathbf{q}(x, y, z; AoA, M) = \sum_{j=1}^{n} A_j(AoA, M)\mathbf{Q}_j(x, y, z), \tag{2}$$

where the POD-modes are the eigenfunctions of the *covariance matrix*, which is defined here as

$$R_{ij} = \langle \mathbf{q}_i, \mathbf{q}_j \rangle \tag{3}$$

in terms of the following inner product, which is consistent with the residual (10),

$$\langle \mathbf{q}_i, \mathbf{q}_j \rangle = \sum_{k=1}^{N_C} \left(\iint_{\Gamma_k} \mathbf{q}_i \, dA \right) \left(\iint_{\Gamma_k} \mathbf{q}_j \, dA \right). \tag{4}$$

Here, Γ_k are the boundaries of N_E elementary cells in the computational domain. If the expansion (2) is truncated to $n \leq N_0$ terms, then the root mean square (RMS), relative error in reconstructing all snapshots, in terms of the norm associated with the inner product (4), is

$$\text{RMS error} = \sqrt{\frac{\sum_{i=n+1}^{N_0} \gamma_i}{\sum_{i=1}^{N_0} \gamma_i}}, \tag{5}$$

where $\gamma_1 \geq \ldots \geq \gamma_{N_0} \geq 0$ are the eigenvalues of the matrix (3). This gives an a priori estimate for truncation of the expansions (2).

III. Derivation of the reduced order model

The still unknown POD amplitudes are calculated minimizing a positive definite residual of the governing equations and boundary conditions, $\mathcal{H}$, which will be a positive functional of the flow variable distributions that only vanishes when both the equations and boundary conditions are identically satisfied. Proceeding in this way involves several difficulties, which will be dealt with in the following sections. In particular:

1) Deciding what equations (either the exact equations, a simplified version of these, or those that are implicit in the CFD solver) should be used to define the residual.
2) Defining the residual using all mesh points in the computational mesh is quite computationally expensive. Instead, a much fewer amount of them, concentrated in a projection window can be used.
3) Dividing the computational domain into subdomains, and applying the method to each subdomain separately, can be convenient when the flow topology in the subdomains is somewhat decoupled.
4) Defining the POD manifold locally in the parameter space decreases the number of POD mode amplitudes.

A. Using the Euler equations in conservative form to calculate the residual

The safest strategy would be to define the residual using the approximate Reynolds averaged Navier Stokes (RANS) equations that are implicit in the CFD solver. But this would make the derivation of the ROM quite involved and the ROM itself dependent of the CFD solver. Instead, we shall take advantage of the fact that the Reynolds number is large to define the residual in terms of the conservative form of the Euler equations. Unlike ROMs based on snapshots calculated by the Euler equations, the ROM is intended to provide the correct vorticity within an approximation comparable to that of the RANS equations. This is because the possible vorticity distributions are already contained in the RANS calculated snapshots. As already noticed by us in a related problem [9],such combined use of the RANS and Euler equations is justified in two steps:

i. RANS equations differ from the exact equations in the turbulence modeling terms and the numerical stabilizers, which are expected to have a small effect on the larger scales. These are accounted for by the most energetic POD modes. Thus, if only the latter are retained, the effect on the unphysical terms in the RANS equations should be small.
ii. Both calculating POD modes and the residual is made adding contributions from the pointwise values of the flow variables in many points in the computational mesh, which involves a spatial averaging. Thus, if the Reynolds number is large, the effect of viscous and thermal conductive terms in both the calculation of the covariance matrix and the residual is small because viscous effects are localized in small spatial regions (boundary layers, shear layers, and shock waves).

In order to maintain the validity of the use of the Euler equations, some care will be taken in subsection III-B below, where a residual will be defined that is based on a few points in a projection window.

A further increase of the computational efficiency will result using the following conservative of the Euler equations in a generic domain Ω,

$$\text{EQ}_1 \equiv \mathcal{A}^{-1} \iint_{\Gamma} \rho \mathbf{v} \cdot \mathbf{n} \, dS = 0, \tag{6}$$

$$\begin{pmatrix} \text{EQ}_2 \\ \text{EQ}_3 \\ \text{EQ}_4 \end{pmatrix} \equiv \mathcal{A}^{-1} \iint_{\Gamma} \left[\frac{\rho \mathbf{v}}{\rho} \rho \mathbf{v} + p\mathbf{I} \right] \cdot \mathbf{n} \, dS = 0, \tag{7}$$

$$\text{EQ}_5 \equiv \mathcal{A}^{-1} \iint_{\Gamma} \left[e\rho \mathbf{v} \cdot \mathbf{n} \right] \, dS = 0, \tag{8}$$

where Γ is the boundary of the domain Ω, $\mathcal{A}$ is the area of Γ, $\mathbf{I}$ is the identity matrix, $\mathbf{n} = (n_x, n_y, n_z)$ is the outward

ISBN: 978-988-19251-5-2
ISSN: 2078-0958 (Print); ISSN: 2078-0966 (Online)

unit normal to Γ, and e is the modified mechanical energy per unit mass, defined as

$$e = \rho^{-2}\left[\rho p + \frac{\gamma-1}{2}(\rho\mathbf{v})\cdot(\rho\mathbf{v})\right]. \tag{9}$$

Equations (6)-(8) apply in any subdomain Ω of the computational domain, namely in any smooth surface Γ contained in the computational domain; and conversely, imposing these equations in all elementary cells in the computational domain, provides a good (finite volume) approximation of the solution. Using this, the residual is defined as

$$\mathcal{H} = \sum_{k=1}^{N_E}\sum_{i=1}^{5}\sqrt{|EQ_i(\Gamma_k)|} + \sum_{m=1}^{N_{BC}}\sum_{i=1}^{5}\sqrt{|BC_i(x_m,y_m,z_m)|}, \tag{10}$$

where BC_i and EQ_i are as defined in (2), (6)-(8), respectively, and in principle the sums are extended to N_E elementary cells and the N_{BC} points in the boundary of the computational mesh. In the following subsections some improvements will be introduced in the residual.

If the expressions inside the square roots in (10) were squared, then a definition more alike to the L_2 norm would be obtained, but such expression would be more sensitive to CFD localized errors, which can be somewhat large. This has been discussed by Alonso *et al.* (see [6], [15]) in a related incompressible fluid dynamics problem, comparing various possible definitions of the residual.

B. Using a few elementary cells in a projection window to calculate the residual and the covariance matrix

As anticipated above, the POD-mode amplitudes are calculated minimizing the function

$$\mathcal{H} = \mathcal{H}(A_1,\ldots,A_n), \tag{11}$$

which is obtained substituting the expansions (2) into (10). The most computationally expensive part of the process is the calculation of the residual, which involves a number of operations comparable to the total number of points ($\sim 3{\cdot}10^6$ in the HTP application below). This computational cost can be reduced noting that: (i) minimizing (11) can be seen as solving n equations, (ii) the residual involves information from N_E elementary cells, and (iii) the total number of elementary cells in the computational domain is selected by the CFD solver to fulfill numerical requirements, while the number of retained modes is related to the true aerodynamic information that is present in the snapshots. Thus, calculating POD modes and the residual does not require information from all mesh points. Instead, the number of surface integrals in (4) and (11) will be taken just somewhat larger than the number of retained modes. The selected elementary cells can be either scattered over the computational domain or concentrated in a projection window. The latter is generally a better choice if the projection window includes the relevant aerodynamic information, subject to only mild limitations:

i. Since the residual is based on the Euler equations, excluding boundary layers is a good choice.
ii. Excluding regions of large concentrated CFD errors is also convenient to avoid the spurious effect of these.

In the application to the HTP below, the O-mesh around the HTP surface will be taken as projection window, excluding both the boundary layer and a portion of the O-mesh near the HTP tip, where CFD errors are concentrated; 208 surface integrals scattered in the resulting projection window will be considered in the computation of both the residual (10) and the inner product (4).

C. Division of the projection window into subdomains

As noticed and explained by [16], the aerodynamic flow near an aircraft part may behave in an independent fashion (as the parameters are varied) in various subdomains of the computational domain. In this case, the number of POD modes needed to describe the complete flow field for a required accuracy is approximately equal to the product of the numbers of modes required in the subdomains. Thus, division into subdomains reduces the effective number of POD modes. As an additional advantage, the resulting process is easily parallelized.

Now, in the HTP application, we note that the suction and pressure sides behave fairly independently of each other as the angle of attack and the Mach number are varied. Thus, we consider two disjoint subdomains in the O-mesh that cover the suction and pressure sides. The boundary between both regions is close to the stagnation point, whose surroundings bear quite important information on the complete flow field and sharp flow variables gradients. This means that the reconstructions in these subdomains may show discontinuities at the common boundary. The latter are smoothed out projecting the reconstructed flow distributions onto a set of POD modes calculated for the whole computational domain.

D. Using a local POD manifold

Local definition of the POD modes in the parameter space reduces the number of required POD modes. Here, at each point of the parameter space, (AoA, M), local modes will be defined applying POD to those snapshots that are closest to the point. This is made in three steps, as follows:

(i) A first approximation, $\tilde{\mathbf{q}}$, of the state vector is obtained using Shepard's interpolation [17] of neighboring snapshots.
(ii) A distance from each snapshot (labeled with the index j) to $\tilde{\mathbf{q}}$ is defined as the orthogonal projection

$$D_j = 1 - \frac{\langle\tilde{\mathbf{q}},\mathbf{q}_j\rangle}{\sqrt{\langle\tilde{\mathbf{q}},\tilde{\mathbf{q}}\rangle}\sqrt{\langle\mathbf{q}_j,\mathbf{q}_j\rangle}}, \tag{12}$$

where the inner product is that used to calculate the POD modes, see eq.(4). The N_1 nearest snapshots are considered, where N_1 must be somewhat large than the required number of POD modes (say, twice as much). Then, a number of POD modes, $\tilde{N}_1$, is selected using the a priori error estimate (5), to keep root mean square errors (RMSE) within a specified bound ϵ_{LM}.
(iii) A safety factor $F > 1$ is defined and the $N_2 = F\tilde{N}_1$ nearest snapshots are retained to evaluate the POD manifold that is finally used to calculate the residual. Note that N_2 can be either smaller or larger than N_1.

The local manifold in each subdomain (see subsection III-C), results from applying POD to the local snapshots, retaining the appropriate number of modes to keep the a priori error estimate (5) smaller than a required error bound ϵ_{GA}.

ISBN: 978-988-19251-5-2
ISSN: 2078-0958 (Print); ISSN: 2078-0966 (Online)

E. Summarizing the ROM derivation method

The method to calculate the flow variables for given values of the parameters proceeds in seven steps:

1. N_0 snapshots are CFD calculated for representative values of the parameters in a given parameter range.
2. Some elementary cells are selected in a projection window (as explained in subsection III-B) to calculate the surface integrals appearing in (10) and (4). The computational domain is divided into various subdomains, as explained in subsection III-C.
3. A local selection of snapshots is made using the algorithm described in subsection III-D. Such selection is performed for each subdomain independently.
4. The flow variables are expanded (in each subdomain) in POD modes as in eq.(2). The POD-mode amplitudes A_i depend on the subdomain but are common to the five flow variables.
5. The number of retained modes within a prescribed accuracy ϵ_{GA} can be obtained using equation (5). An initial guess for the amplitudes values is obtained via POD plus interpolation.
6. The amplitudes are calculated in each subdomain minimizing the residual (10) with a genetic algorithm (GA).
7. The state variables are reconstructed in each subdomain of the projection window using their associated set of amplitudes. The flow field in the whole computational domain is obtained merging the solutions in the various subdomains as explained in subsection III-C, and projecting the resulting merged solution onto a set of most energetic global POD modes, obtained in the whole computational domain applying POD to the complete set of N_0 snapshots.

IV. Results

Let us now check the ability of the method developed in last section to provide the aerodynamic flow around the HTP described in section II. The various parameters of the method (which have been left free in the description above) are chosen after some calibration for the HTP as follows:

- The upper bounds of the RMSE required to chose the number of modes and the dimension of the local manifold are $\epsilon_{GA} = \epsilon_{LM} = 10^{-3}$; the initial guess of the dimension of the local manifold and the safety factor used in subsection III-D are $N_1 = 40$ and F = 2.5, respectively.
- The GA parameters are as follows. The total number of individuals is 10,000, with a discretization of 10 bits per POD-mode amplitude of each individual; the span allowed around the POD+I initial solution equals 50%, and 2% of elite individuals that go straight into the next generation. The crossover probability is equal to 0.8 and 5,000 bits are mutated in each generation. Convergence is acheived if the residual remains constant along 100 generations.

Using the ELSA code, 117 snapshots have been calculated at all combinations of the 13 equispaced values of the angle of attack and the 9 equispaced values of the Mach number indicated in Fig.2. In addition, the 28 test points (indicated in in Fig.2 will be used to test the performance of the ROM. These are denoted as PTX_1X_2, where $X_1 = 1, \ldots, 8$ labels

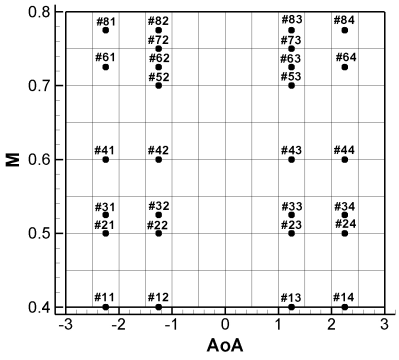

Fig. 2. The parameter space, with the test points (filled circles) and the snapshots in combination #1 (cross points of the net).

the following values of the Mach number $M = 0.4$, 0.5, 0.525, 0.6, 0.7, 0.725, 0.75, and 0.775, and $X_2 = 1, \ldots, 4$ labels the following values of the angle of attack $-2.25°$, $-1.25°$, $1.25°$ and $2.25°$; note that not all combinations of these values of M and AoA are considered.

Three combinations of snapshots will be used to calculate the POD manifold:

- *Combination* #1 consists of the whole set of 117 calculated snapshots.
- *Combination* #2 contains the $(7 \times 5 =)$ 35 snapshots resulting from reducing in combination #2 the 9 cases in the Mach number to the 5 equispaced values between 0.4 and 0.8.
- *Combination* #3 contains the $(5 \times 5 =)$ 25 snapshots resulting from reducing in combination #2 the 13 cases in the Mach number to the 5 equispaced values between $-3°$ and $3°$.

The ROM provides the flow variable distributions in the whole computational domain. Such distributions allow for calculating any property of the aerodynamic flow. The ability of the ROM to provide load distributions is checked considering the lift, pressure drag, and lateral force coefficients, defined in terms of surface integrals over the HTP surface as

$$(C_L, C_{PD}, C_y) = \iint_{S_{HTP}} (n_L, n_{PD}, n_y) C_p \, dS \qquad (13)$$

where $\mathbf{n} = (n_x, n_y, n_z)$ is the outward unit wall normal to the HTP surface, S_{HTP}, $n_L = -n_x \sin AoA + n_z \cos AoA$, $n_{PD} = n_x \cos AoA + n_z \sin AoA$, and C_p is the pressure coefficient, defined as

$$C_p = 2\frac{p-1}{\gamma M^2} \qquad (14)$$

in terms of the specific heat ratio, γ. Similarly, the roll, pitch, and yaw moment coefficients are defined as

$$(C_R, C_M, C_N) = -\iint_{S_{HTP}} (\mathbf{x} - \mathbf{x}_0) \times \mathbf{n} C_p \, dS \qquad (15)$$

where $\mathbf{x} = (x, y, z)$ is the position vector and $\mathbf{x}_0 = (0.25, 0, 0)$ is the reference point to calculate moments.

The RMS and maximum errors of the reconstructed aerodynamic coefficients are shown table I. The first two columns show the errors resulting from calculating the residual and the

ISBN: 978-988-19251-5-2
ISSN: 2078-0958 (Print); ISSN: 2078-0966 (Online)

	#1 O-mesh	#1 reduced	#2 reduced	#3 reduced
C_L	0.39(1.06)	0.40 (1.28)	1.40 (2.76)	2.18 (6.39)
C_{PD}	4.62(12.77)	4.85 (14.49)	4.96 (11.12)	7.17 (18.05)
C_Y	2.01(5.81)	2.05 (5.93)	2.34 (5.80)	2.97 (7.43)
C_M	0.30(0.73)	0.28 (0.84)	1.00 (2.00)	1.47 (3.74)
C_R	0.37(0.97)	0.39 (1.17)	1.32 (2.59)	2.07 (5.90)
C_N	4.12(11.93)	4.31 (13.02)	2.09 (4.80)	4.10 (7.90)

TABLE I
RMS ERRORS (IN %) IN THE 28 TEST POINTS RESULTING FROM CALCULATING THE SIX AERODYNAMIC COEFFICIENTS WITH THE THREE COMBINATIONS OF SNAPSHOTS; MAXIMUM ERRORS ARE ALSO GIVEN IN PARENTHESIS.

	#1	#2	#3
ρu	0.38(0.01)	0.60(0.03)	1.02(0.03)
ρv	0.40(0.00)	0.60(0.00)	0.93(0.00)
ρw	0.18(0.14)	0.22(0.25)	0.31(0.27)
ρ	0.23(0.01)	0.30(0.02)	0.40(0.02)
p	0.25(0.01)	0.33(0.02)	0.42(0.02)

TABLE II
RMS ERRORS (IN %) OF THE FLOW VARIABLESIN THE O-MESH FOR THE FIVE COMBINATIONS OF SNAPSHOTS; RMS ERRORS IN THE WHOLE COMPUTATIONAL MESH ARE GIVEN IN PARENTHESIS.

covariance matrix using all elementary cells in the O-mesh (first column) and 208 of them (second column). Note that errors are comparable. The two combinations of snapshots are compared (using 208 elementary cells) in the remaining columns, which show that:

1) The errors resulting from using the whole O-mesh and 208 surface integrals are comparable.
2) The errors in C_{PD}, C_Y, and C_N are larger than the errors in the remaining coefficients, which is due to the fact that their actual values of these coefficients are smaller than the remaining coefficients.
3) Maximum errors are at most three times larger than the RMS counterparts.
4) Combination #1 generally yields better results than ccombination #2, and this provides smaller errors than combination #3, which was to be expected. It is remarkable that combination #3 provides results that are good enough in industrial applications.
5) It is clear that if the snapshots were appropriately located in in the parameter space, then the results would further improve using a smaller number of snapshots, reducing the required CPU time. This is important since POD+GA calculations are quite fast compared to the CFD calculation of the snapshots, which is by far the slowest part of the process.

In order to compare (both in the O-mesh and in the whole computational domain) the results provided by the various combinations of snapshots on the whole aerodynamic flow, the RMS error in each variable for the 28 test points are considered. The RMSE is defined as

$$\text{RMSE} = \sqrt{\frac{1}{28\langle 1,1\rangle}\sum_{k=1}^{28}\langle E_k, E_k\rangle} \qquad (16)$$

where Ω is either the O-mesh around the HTP or the whole computational domain and the pointwise error is defined for

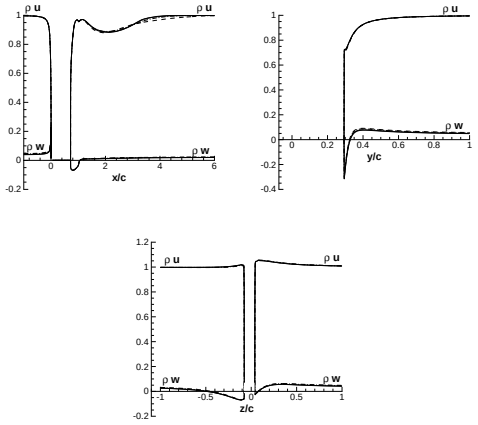

Fig. 3. ρu and ρw (thick and thin lines, respectively) along the lines $y = 0, z = 0$ (up-left), $x = 0, z = 0$ (up-right), and $x = 0, y = 0$ (down) at test point PT84. CFD and ROM results using combinations #1 and #6 are plotted using solid, dashed, and dot-dashed lines, respectively.

each flow variable ϕ as

$$E(x,y,z) = \frac{|\phi_{\text{CFD}}(x,y,z) - \tilde{\phi}_{\text{ROM}}(x,y,z)|}{\max|\phi_{\text{CFD}}|}. \qquad (17)$$

Here, the subscripts CFD and ROM refer to the CFD and ROM approximations, respectively, and $\max|\phi_{\text{CFD}}|$ denotes the maximum, absolute (CFD) value of the flow variable in Ω.

Results on the flow variables distribution are given in terms of RMS errors in table II and show that:

1) The RMS errors in the O-mesh are always larger than their counterparts in the whole computational domain.
2) The larger the number of snapshots, the better the results.
3) RMS errors are below 1% for all the combinations, which is more than enough in most industrial applications.

In order to illustrate the approximation of the aerodynamic field in the whole computational domain, three distributions of the pressure are shownin Fig.3 along the indicated straight lines, as calculated using combinations #1 and #5. Note that the approximation is quite good (ROM and CFD results are plot indistinguishable) except for some small discrepancies in the wake. This is a quite strong result, taking into account that the ROM was constructed from aerodynamic information on a limited set of points near the HTP surface, which did not included the wake, and confirms that the wake is somewhat slaved to the upstream flow topology. In addition, the reconstruction of the aerodynamic field in the boundary layer near the HTP surface is illustrated in Fig. 4, considering the test point PT84. In this figure, the x-velocity is plotted vs. the wall-normal co-ordinate at four representative points on the HTP surface. Note that the results are quite good (CFD and ROM results are almost indistinguishable) in three of the points (cases (a), (b), and (d)). This is because these three points are not in a vicinity of a shock wave. The fact that these results are so good could be seen as surprising at first sight because ROM calculations were based on the Euler equations, which do not apply in the boundary layer. The reason is that the boundary layer structure is somewhat

ISBN: 978-988-19251-5-2
ISSN: 2078-0958 (Print); ISSN: 2078-0966 (Online)

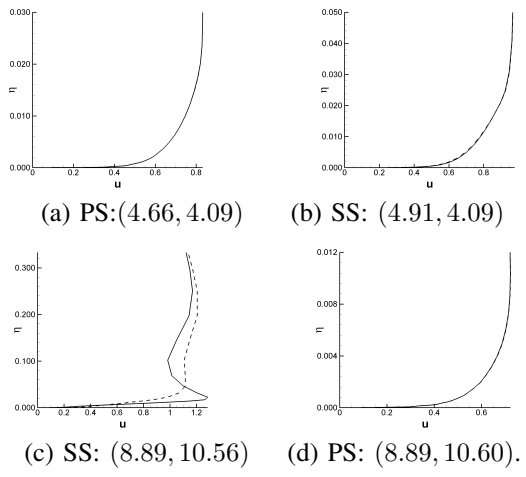

(a) PS:$(4.66, 4.09)$ (b) SS: $(4.91, 4.09)$

(c) SS: $(8.89, 10.56)$ (d) PS: $(8.89, 10.60)$.

Fig. 4. x-velocity distribution calculated for PT84 using combination #1 along the wall-normal co-ordinate in the boundary layer at four points (x, y) on the HTP surface, as indicated. PS and SS refer to the pressure and suction sides, respectively. CFD and ROM results are plotted using solid and dashed lines, respectively.

slaved (along the wall-normal direction) to the outer flow. Thus, if the latter is well calculated (which occurs if no nearby shock wave is present), then the boundary layer is well approximated too, since the correct coupling between both is present in the CFD calculated snapshots. Case (c) instead corresponds to a point that is under a shock wave, and the approximation is just reasonable.

V. Concluding Remarks

A method has been developed to construct ROMs of three dimensional, steady aerodynamic fields of industrial interest depending on various parameters. The method is based on the calculation of various aerodynamic fields (called the snapshots), for representative parameter values. The CFD solver is a typical RANS solver used in the aeronautic industry. The ROM is constructed minimizing a properly defined residual based on the governing equations and boundary conditions. The method has been tested considering the aerodynamic field around a commercial aircraft horizontal tail plane, depending on two parameters, the Mach number and the angle of attack, in a range that included transonic flows. Various improvements have been presented to improve computational efficiency:

- It is the conservative Euler equations and not the RANS equations that are used to calculate the residual. This makes the method independent of the turbulence model/numerical stabilizers that might have been used.
- Both the residual and the covariance matrix of the snapshots set are calculated using only a limited number of mesh points that are concentrated in a projection window. This strongly improves the computational cost maintaining precision, provided that the projection window includes relevant aerodynamic information. Localized CFD errors can be avoided excluding them from the projection window.
- Residual minimization was made using a genetic algorithm. Computational efficiency would be further improved using faster gradient-like methods, which is the object of current research.
- The POD manifold can be defined locally in the parameter space, and calculations can be made in various subdomains of the projections window, which makes the method quite flexible.
- In spite of these simplifications, the method provides quite good approximations in the whole computational domain, including the boundary layers and the wake.
- Location of the snapshots in the parameter space is very important, which suggests that a method to select the snapshots position would further increase the computational efficiency. Again, this is currently under research.

The reduced order model developed above has been designed keeping in mind its industrial use, which would improve the somewhat rough, ad hoc methods that are used nowdays in industry to cope with multiparameter aerodynamic flows.

References

[1] B. Galletti, C. Bruneau, C. Zannetti, and A. Iollo, "Low-order modelling of laminar flow regimes past a confined square cylinder," *J. Fluid Mech.*, vol. 503, pp. 161–170, 2004.

[2] S. Sirisup and G. Karniadakis, "A spectral viscosity method for correcting the long term behaviour of pod models," *J. Comput. Phys.*, vol. 194, pp. 92–116, 2004.

[3] J. Burkhard, M. Gunzburger, and H. Lee, "Pod and cvt based reduced order modeling of navier-stokes flows," *Comput. Method. Appl. Mech. Engrg.*, vol. 196, pp. 337–355, 2006.

[4] M. Rapun and J. Vega, "Reduced order models based on local pod plus galerkin projection," *J. Comput. Phys.*, vol. 229, pp. 3046–3063, 2010.

[5] P. LeGresley and J. Alonso, "Investigation of nonlinear projection for pod based reduced order models for aerodynamics," in *AIAA 2001-16737, 39th Aerospace Science Meeting & Exhibit*, January.

[6] D. Alonso, A. Velazquez, and J. Vega, "Robust reduced order modeling of heat transfer in a back step flow," *Int. J. Heat Mass Tran.*, vol. 52, pp. 1149–1157, 2009.

[7] Y. Rouizi, J. Favennec, Y. Ventura, and D. Petit, "Numerical model reduction of 2d steady incompressible laminar flow: application on the flow over a backward facing step," *J. Comput. Phys.*, vol. 228, pp. 2239–2255, 2009.

[8] E. Bache, J. Vega, and A. Velazquez, "Model reduction in fluid-thermal problems with variable geometry," *Int. J. Therm. Sci.*, vol. 49, pp. 2376–2384, 2010.

[9] D. Alonso, J. Vega, and A. Velazquez, "Reduced order model for viscous aerodynamic flow past an airfoil," *AIAA J.*, vol. 48, pp. 1946–1958, 2010.

[10] L. Cambier and M. Gazaix, "ELSA: An efficient object-oriented solution to CFD complexity." *AIAA Paper*, no. 02-0108, 2002.

[11] S. Ben Kheli, J. Gervois, G. Carrier, F. Moens, and P. Viscat, "Assessment of ELSA software through civil transport aircraft configurations." CEAS Aerospace Aerodynamics Research Conference. Cambridge, UK., Tech. Rep., January 2002.

[12] J. Tannehill, D. Anderson, and R. Pletcher, *Computational Fluid Mechanics and Heat Transfer*. Taylor & Francis., 1997.

[13] J. Edwards and S. Chandra, "Comparison of eddy viscosity transport turbulence models for three dimensional, shock separated flow fields," *AIAA J.*, vol. 34, no. 4, pp. 756–763, 1996.

[14] P. Spalart and S. Allmaras, "A one-equation turbulence model for aerodynamic flows," *AIAA Paper*, no. 92-0439, 1992.

[15] D. Alonso, A. Velazquez, and J. Vega, "A method to generate computationally efficient reduced order models," *Comput. Method. Appl. Mech. Engrg.*, vol. 198, pp. 2683–2691, 2009.

[16] L. Lorente, J. Vega, and A. Velazquez, "Compression of aerodynamic databases using high order singular value decomposition," *Aerosp. Sci. Technol.*, vol. In Press, Uncorrected Proof, 2009.

[17] D. Shepard, "A two-dimensional interpolation function for irregularly-spaced data," Proceedings of the 1968 ACM National Conference, Tech. Rep., 1968.

ISBN: 978-988-19251-5-2
ISSN: 2078-0958 (Print); ISSN: 2078-0966 (Online)